Eur. Phys. J. C (2018) 78:498
https://doi.org/10.1140/epjc/s10052-018-5963-1

THE EUROPEAN PHYSICAL JOURNAL C

Regular Article - Theoretical Physics

Precise determination of $\alpha_S(M_Z)$ from a global fit of energy–energy correlation to NNLO+NNLL predictions

Adam Kardos[1], **Stefan Kluth**[2], **Gábor Somogyi**[3], **Zoltán Tulipánt**[1], **Andrii Verbytskyi**[2,a]

[1] Institute of Physics, University of Debrecen, PO Box 105, Debrecen 4010, Hungary
[2] Max-Planck-Institut für Physik, Föringer ring 6, 80805 Munich, Germany
[3] MTA-DE Particle Physics Research Group, University of Debrecen, PO Box 105, Debrecen 4010, Hungary

Received: 7 May 2018 / Accepted: 31 May 2018 / Published online: 15 June 2018

Abstract We present a comparison of the computation of energy–energy correlation in e^+e^- collisions in the back-to-back region at next-to-next-to-leading logarithmic accuracy matched with the next-to-next-to-leading order perturbative prediction to LEP, PEP, PETRA, SLC and TRISTAN data. With these predictions we perform an extraction of the strong coupling constant taking into account non-perturbative effects modelled with Monte Carlo event generators. The final result at NNLO+NNLL precision is $\alpha_S(M_Z) = 0.11750 \pm 0.00018(exp.) \pm 0.00102(hadr.) \pm 0.00257(ren.) \pm 0.00078(res.)$.

1 Introduction

The strong interaction in the Standard Model (SM) is described by quantum chromodynamics (QCD) [1–4]. The theory successfully models the interactions between quarks and gluons and is a source of numerous predictions. Verifying the predictions of QCD is instrumental for searches for physics beyond the SM at the LHC, since the reliable prediction of SM processes as sources of backgrounds for searches is essential.

Precision measurements of event shape distributions in e^+e^- annihilation have provided detailed experimental tests of QCD and remain one of the most precise tools used for extracting the strong coupling α_S from data [5,6]. Quantities related to three-jet events are particularly well suited for this task.

The state of the art for QCD for event shape observables currently includes exact fixed-order next-to-next-to-leading order (NNLO) corrections for the six standard three-jet event shapes of thrust, heavy jet mass, total and wide jet broadening, C-parameter and the two-to-three jet transition variable y_{23} [7–9] as well as jet cone energy fraction [9], oblateness and energy–energy correlation [10]. The numerical matrix element integration codes described in the references allow the straightforward computation of any suitable, i.e. collinear and infrared safe event shape or jet observable.

However, fixed-order predictions have a limited kinematical range of applicability. For small values of an event shape observable y corresponding to events with two-jet-like topologies the fixed-order predictions do not converge well. This is due to terms where each power of the strong coupling α_S^n is enhanced by a factor $(\ln y)^{n+1}$ (leading logs), $(\ln y)^n$ (next-to-leading logs) etc. For three-jet event shapes such logarithmically enhanced terms can be resummed at next-to-next-to-leading logarithmic (NNLL) accuracy [11–17], i.e. up to terms $\sim (\ln y)^{n-1}$. Resummation in next-to-next-to-next-to-leading logarithmic (N^{3}LL) accuracy has been achieved for the C-parameter [18] and thrust [19]. A prediction incorporating the complete perturbative knowledge about the observable can be derived by matching the fixed-order and resummed calculations.

For the frequently used event shapes of thrust, heavy jet mass, total and wide jet broadening, C-parameter and y_{23}, NNLO predictions matched to NLL resummation were presented in [20]. Predictions at NNLO matched to N^{3}LL resummation are also known for thrust [12,19] and the C-parameter [18].

In this paper we consider the energy–energy correlation (EEC) in e^+e^- annihilation and present NNLO predictions matched to NNLL resummation for the back-to-back region. EEC was the first event shape for which a complete NNLL resummation was performed [11] while the fixed-order NNLO corrections to this observable were computed recently [10]. Moreover, EEC is the first event shape observable for which an analytic fixed-order NLO correction was computed [21].

[a] e-mail: andrii.verbytskyi@mpp.mpg.de

The agreement between the predictions at NNLO+NNLL accuracy and the measured data is still not perfect. The discrepancy can be attributed mainly to non-perturbative hadronization corrections. We extract these corrections from data by comparison to state-of-the-art Monte Carlo predictions and determine the value of the strong coupling by comparing our results to measurements over a wide range of centre-of-mass energies. Our analysis allows us to target the highest precision of α_S determination and we present the first global fit of the strong coupling to EEC at NNLO+NNLL accuracy. Our analysis also represents the first extraction of α_S based on Monte Carlo hadronization corrections obtained from NLO Monte Carlo setups at NNLO+NNLL precision.

2 EEC distribution in perturbation theory

EEC is the normalized energy-weighted cross section defined in terms of the angle between two particles i and j in an event [22]:

$$\frac{1}{\sigma_t}\frac{\mathrm{d}\Sigma(\chi)}{\mathrm{d}\cos\chi} \equiv \frac{1}{\sigma_t}\int \sum_{i,j}\frac{E_i E_j}{Q^2}\mathrm{d}\sigma_{e^+e^-\to ij+X}\,\delta(\cos\chi-\cos\theta_{ij}), \quad (1)$$

where E_i and E_j are the particle energies, Q is the centre-of-mass energy, $\theta_{ij}=\chi$ is the angle between the two particles and σ_t is the total hadronic cross section. The back-to-back region $\theta_{ij}\to 180^\circ$ corresponds to $\chi\to\pi$, while the normalization ensures that the integral of the EEC distribution from $\chi=0^\circ$ to $\chi=180^\circ$ is unity.[1]

2.1 Fixed-order and resummed calculations

The differential EEC distribution has been computed numerically at NLO accuracy in perturbation theory some time ago [24–34] and efforts towards obtaining an analytic result at this order [35,36] have culminated in a complete calculation very recently [21]. The NNLO prediction has also been obtained in ref. [10] using the CoLoRFulNNLO method [9,37,38]. At the default renormalization scale[2] of $\mu=Q$ the fixed-order prediction reads

$$\left[\frac{1}{\sigma_0}\frac{\mathrm{d}\Sigma(\chi,Q)}{\mathrm{d}\cos\chi}\right]_{\text{f.o.}} = \frac{\alpha_S(Q)}{2\pi}\frac{\mathrm{d}A(\chi)}{\mathrm{d}\cos\chi} + \left(\frac{\alpha_S(Q)}{2\pi}\right)^2\frac{\mathrm{d}B(\chi)}{\mathrm{d}\cos\chi} + \left(\frac{\alpha_S(Q)}{2\pi}\right)^3\frac{\mathrm{d}C(\chi)}{\mathrm{d}\cos\chi} + \mathcal{O}(\alpha_S^4), \quad (2)$$

where A, B and C are the perturbative coefficients at LO, NLO and NNLO, normalized to the LO cross section for $e^+e^-\to$ hadrons, σ_0. In massless QCD this normalization cancels all electroweak coupling factors, and the dependence on the collision energy enters only through $\alpha_S(Q)$. However, experiments measure the distribution normalized to the total hadronic cross section, so physical predictions must be normalized to σ_t. The distribution normalized to the total hadronic cross section can be obtained from the expansion in Eq. (2) through multiplying by σ_0/σ_t. For massless quarks, this ratio is independent of all electroweak couplings and reads

$$\frac{\sigma_0}{\sigma_t} = 1-\frac{\alpha_S(Q)}{2\pi}A_t + \left(\frac{\alpha_S(Q)}{2\pi}\right)^2\left(A_t^2-B_t\right)+\mathcal{O}(\alpha_S^3),$$

with

$$A_t = \frac{3}{2}C_F$$

and

$$B_t = C_F\left[\left(\frac{123}{8}-11\zeta_3\right)C_A - \frac{3}{8}C_F - \left(\frac{11}{2}-4\zeta_3\right)n_f T_R\right].$$

The colour factors which appear above are given by

$$C_A = 2N_c T_R,\quad C_F=\frac{N_c^2-1}{N_c}T_R \quad\text{and}\quad T_R=\frac{1}{2},$$

while n_f denotes the number of light quark flavours.

The renormalization scale dependence of the fixed-order prediction can be restored using the renormalization group equation for α_S and one finds

$$\left[\frac{1}{\sigma_t}\frac{\mathrm{d}\Sigma(\chi,\mu)}{\mathrm{d}\cos\chi}\right]_{\text{f.o.}} = \frac{\alpha_S(\mu)}{2\pi}\frac{\mathrm{d}\bar{A}(\chi,x_R)}{\mathrm{d}\cos\chi} + \left(\frac{\alpha_S(\mu)}{2\pi}\right)^2\frac{\mathrm{d}\bar{B}(\chi,x_R)}{\mathrm{d}\cos\chi} + \left(\frac{\alpha_S(\mu)}{2\pi}\right)^3\frac{\mathrm{d}\bar{C}(\chi,x_R)}{\mathrm{d}\cos\chi} + \mathcal{O}(\alpha_S^4), \quad (3)$$

where

$$\begin{aligned}
\bar{A}(\chi,x_R) &= A(\chi),\\
\bar{B}(\chi,x_R) &= B(\chi) + \left(\frac{1}{2}\beta_0\ln(x_R^2)-A_t\right)A(\chi),\\
\bar{C}(\chi,x_R) &= C(\chi) + \left(\beta_0\ln(x_R^2)-A_t\right)B(\chi)\\
&\quad + \left(\frac{1}{4}\beta_1\ln(x_R^2)+\frac{1}{4}\beta_0^2\ln^2(x_R^2)-A_t\beta_0\ln(x_R^2)\right.\\
&\quad \left.+A_t^2-B_t\right)A(\chi),
\end{aligned}$$

[1] Refs. [11] and [23] use the opposite convention of $\theta_{ij}=180^\circ-\chi$ such that the back-to-back region corresponds to $\chi\to 0^\circ$. Here we use $\theta_{ij}=\chi$ throughout which agrees with the experimental convention.

[2] We use the $\overline{\text{MS}}$ renormalization scheme throughout the paper.

with $x_R = \mu/Q$. Finally, using three-loop running the scale dependence of the strong coupling is given by

$$\alpha_S(\mu) = \frac{4\pi}{\beta_0 t}\left[1 - \frac{\beta_1}{\beta_0^2 t}\ln t + \left(\frac{\beta_1}{\beta_0^2 t}\right)^2\left(\ln^2 t - \ln t - 1 + \frac{\beta_0\beta_2}{\beta_1^2}\right)\right].$$

Here, $t = \ln(\mu^2/\Lambda^2_{\rm QCD})$ and the β_i are the $\overline{\rm MS}$-scheme coefficients of the QCD beta function,

$$\begin{aligned}\beta_0 &= \frac{11C_A}{3} - \frac{4n_f T_R}{3},\\ \beta_1 &= \frac{34}{3}C_A^2 - \frac{20}{3}C_A T_R n_f - 4C_F T_R n_f,\\ \beta_2 &= \frac{2857}{54}C_A^3 - \left(\frac{1415}{27}C_A^2 + \frac{205}{9}C_A C_F - 2C_F^2\right)T_R n_f\\ &\quad + \left(\frac{158}{27}C_A + \frac{44}{9}C_F\right)T_R^2 n_f^2.\end{aligned}$$

The fixed-order perturbative predictions diverge for both small and large values of χ, due to the presence of large logarithmic contributions of infrared origin. Concentrating on the back-to-back region $\chi \to 180°$, these contributions take the form $\alpha_S^n \log^{2n-1} y$, where

$$y = \cos^2\frac{\chi}{2}.$$

As y decreases, the logarithms become large and invalidate the use of the fixed-order perturbative expansion. In order to obtain a description of EEC in this limit, the logarithmic contributions must be resummed to all orders. This resummation has been computed at NNLL accuracy in Ref. [11][3] while in Ref. [40] a factorization theorem for EEC was derived based on soft-collinear effective theory which will allow to preform the resummation at N^{3}LL accuracy once the corresponding NNLO jet function is computed. Since the complete jet function is currently not available, we use the NNLL results and formalism of Ref. [11] in the following. The resummed prediction at the default scale of $\mu = Q$ can be written as

$$\left[\frac{1}{\sigma_t}\frac{{\rm d}\Sigma(\chi, Q)}{{\rm d}\cos\chi}\right]_{\rm res.} = \frac{Q^2}{8}H(\alpha_S(Q)) \times \int_0^\infty {\rm d}b\, b\, J_0(b\,Q\sqrt{y})S(Q,b). \quad (4)$$

[3] Note that the NNLL $A^{(3)}$ coefficient in Ref. [11] is incomplete. The full coefficient has been derived in Ref. [39].

The large logarithmic corrections are exponentiated in the Sudakov form factor,

$$S(Q,b) = \exp\left\{-\int_{b_0^2/b^2}^{Q^2}\frac{{\rm d}q^2}{q^2}\left[A(\alpha_S(q^2))\ln\frac{Q^2}{q^2} + B(\alpha_S(q^2))\right]\right\}. \quad (5)$$

The zeroth order Bessel function J_0 in Eq. (4) and $b_0 = 2e^{-\gamma_E}$ in Eq. (5) have a kinematic origin. The functions A, B (not to be confused with the fixed-order expansion coefficients appearing in Eq. (2)) and H in Eqs. (4) and (5) are free of logarithmic corrections and can be computed as perturbative expansions in α_S,

$$A(\alpha_S) = \sum_{n=1}^\infty\left(\frac{\alpha_S}{4\pi}\right)^n A^{(n)}, \quad (6)$$

$$B(\alpha_S) = \sum_{n=1}^\infty\left(\frac{\alpha_S}{4\pi}\right)^n B^{(n)}, \quad (7)$$

$$H(\alpha_S) = 1 + \sum_{n=1}^\infty\left(\frac{\alpha_S}{4\pi}\right)^n H^{(n)}. \quad (8)$$

Explicit expressions for the expansion coefficients (up to NNLL accuracy) in our normalization conventions can be found in Ref. [23].

It is possible to perform the q^2 integration in Eq. (5) analytically and the Sudakov form factor can be written as

$$S(Q,b) = \exp[Lg_1(a_S\beta_0 L) + g_2(a_S\beta_0 L) + a_S g_3(a_S\beta_0 L) + \ldots], \quad (9)$$

where $a_S = \alpha_S(Q)/(4\pi)$ and $L = \ln(Q^2b^2/b_0^2)$ corresponds to $\ln y$ at large b (the $y \ll 1$ limit corresponds to $Qb \gg 1$ through a Fourier transformation). Writing the Sudakov form factor this way clearly shows that $S(Q,b)$ depends on its variables only through the dimensionless combination $b\,Q$. The functions g_1, g_2 and g_3 correspond to the LL, NLL and NNLL contributions. Their explicit expressions can be found in Refs. [11,23].

So far, we have not considered the dependence of the resummed prediction on the renormalization scale. Besides the replacement of $\alpha_S(Q)$ by $\alpha_S(\mu)$ in Eqs. (4) and (9), the resummation functions $g_i(\lambda)$ also acquire renormalization scale dependence,

$$\begin{aligned}g_1(\lambda, x_R) &= g_1(\lambda),\\ g_2(\lambda, x_R) &= g_2(\lambda) + \lambda^2 g_1'(\lambda)\ln(x_R^2),\end{aligned}$$

$$g_3(\lambda, x_R) = g_3(\lambda) + \left[\frac{\beta_1}{\beta_0}\lambda^2 g_1'(\lambda) + \beta_0\lambda g_2'(\lambda)\right]\ln(x_R^2) + \left[\frac{\beta_0}{2}\lambda^3 g_1''(\lambda) + \beta_0\lambda^2 g_1'(\lambda)\right]\ln^2(x_R^2),$$

where the prime denotes differentiation with respect to λ.

The factorization between the constant and logarithmic terms $H(\alpha_S)$ and $S(Q, b)$ in Eq. (4) also involves some arbitrariness, since the argument of the large logarithm L can always be rescaled as

$$L = \ln(Q^2b^2/b_0^2) = \ln(x_L^2 Q^2 b^2/b_0^2) - \ln(x_L^2),$$

provided that x_L is independent of b and that $x_L = \mathcal{O}(1)$ when $Qb \gg 1$. This arbitrariness is parametrized by x_L, which plays a role in the resummed computation which is analogous to the role played by the renormalization scale in the fixed-order calculation. This rescaling of the logarithm introduces some modifications of the resummed formulae and the expansion coefficients in Eqs. (6)–(8). We find

$$\begin{aligned}
\tilde{A}^{(n)}(x_L) &= A^{(n)},\\
\tilde{B}^{(n)}(x_L) &= B^{(n)} - A^{(n)}\ln(x_L^2),\\
\tilde{H}^{(1)}(x_L) &= H^{(1)} - \beta_0 g_2'(0)\ln(x_L^2) + \beta_0 g_1'(0)\ln^2(x_L^2),
\end{aligned}$$

while the Sudakov form factor in Eq. (9) is also modified as follows

$$\begin{aligned}
S(Q, b, x_R, x_L) &= \exp\\
&\times\left[\tilde{L}g_1\left(a_S\beta_0\tilde{L}, \frac{x_R}{x_L}\right) + g_2\left(a_S\beta_0\tilde{L}, \frac{x_R}{x_L}\right)\right.\\
&\left.+\alpha_S g_3\left(a_S\beta_0\tilde{L}, \frac{x_R}{x_L}\right) + \cdots\right],
\end{aligned} \tag{10}$$

where $\tilde{L} = \ln(x_L^2 Q^2 b^2/b_0^2)$.

2.2 Matching the fixed-order and resummed predictions

In order to obtain a prediction which is valid over a wide kinematical range[4] the fixed-order and resummed calculations must be matched. Here we employ the log-R matching scheme as worked out for EEC in Ref. [23], and limit ourselves to recalling the final results.

In the log-R matching scheme for EEC we consider the cumulative distribution

$$\begin{aligned}
\frac{1}{\sigma_t}\widetilde{\Sigma}(\chi, \mu) &\equiv \frac{1}{\sigma_t}\int_0^{\chi} \mathrm{d}\chi'\,(1-\cos\chi')\frac{\mathrm{d}\Sigma(\chi', \mu)}{\mathrm{d}\chi'}\\
&= \frac{1}{\sigma_t}\int_0^{y(\chi)} \mathrm{d}y'\,2(1-y')\frac{\mathrm{d}\Sigma(y', \mu)}{\mathrm{d}y'}.
\end{aligned} \tag{11}$$

The differential EEC distribution is easily recovered from $\widetilde{\Sigma}(\chi, \mu)$,

$$\frac{1}{\sigma_t}\frac{\mathrm{d}\Sigma(\chi, \mu)}{\mathrm{d}\chi} = \frac{1}{1-\cos\chi}\frac{\mathrm{d}}{\mathrm{d}\chi}\left[\frac{1}{\sigma_t}\widetilde{\Sigma}(\chi, \mu)\right].$$

The particular linear combination of moments introduced in Eq. (11) has the property that the divergence of the differential EEC distribution in the forward region ($\chi \to 0$) is suppressed by the factor of $(1 - \cos\chi)$. Hence, in contrast to EEC itself, the fixed-order cumulative coefficients of $\widetilde{\Sigma}(\chi, \mu)$ can be computed reliably. Furthermore, one can show that in massless QCD this cumulative distribution is unity when $\chi = 180°$. Hence, we can integrate the fixed-order differential distribution in Eq. (3) and use the unitarity constraint $\widetilde{\Sigma}(\pi, \mu)/\sigma_t = 1$ to all orders in α_S to fix the constants of integration,

$$\begin{aligned}
\left[\frac{1}{\sigma_t}\widetilde{\Sigma}(\chi, \mu)\right]_{\text{f.o.}} &= 1 + \frac{\alpha_S(\mu)}{2\pi}\bar{\mathcal{A}}(\chi, x_R)\\
&+\left(\frac{\alpha_S(\mu)}{2\pi}\right)^2\bar{\mathcal{B}}(\chi, x_R)\\
&+\left(\frac{\alpha_S(\mu)}{2\pi}\right)^3\bar{\mathcal{C}}(\chi, x_R) + \mathcal{O}(\alpha_S^4).
\end{aligned} \tag{12}$$

Moreover, starting from Eq. (4) and using the definition of $\widetilde{\Sigma}$, Eq. (11), we obtain the following expression for the resummed prediction[5]:

$$\begin{aligned}
\left[\frac{1}{\sigma_t}\widetilde{\Sigma}(\chi, \mu)\right]_{\text{res.}} &= H(\alpha_S(\mu))\int_0^{\infty}\left[Q\sqrt{y}(1-y)J_1(b\,Q\sqrt{y})\right.\\
&\left.+\frac{2y}{b}J_2(b\,Q\sqrt{y})\right]S(Q, b)\mathrm{d}b,
\end{aligned} \tag{13}$$

where the Sudakov form factor $S(Q, b)$ is the one given in Eq. (9).

The final expression for the matched prediction was derived in Ref. [23] and reads

$$\begin{aligned}
\ln\left[\frac{1}{\sigma_t}\widetilde{\Sigma}(\chi, \mu)\right] &= \ln\left\{\frac{1}{H(\alpha_S(\mu))}\left[\frac{1}{\sigma_t}\widetilde{\Sigma}(\chi, \mu)\right]_{\text{res.}}\right\}\\
&-\ln\left\{\frac{1}{H(\alpha_S(\mu))}\left[\frac{1}{\sigma_t}\widetilde{\Sigma}(\chi, \mu)\right]_{\text{res.}}\right\}_{\text{f.o.}}\\
&+\frac{\alpha_S(\mu)}{2\pi}\bar{\mathcal{A}}(\chi, \mu)\\
&+\left(\frac{\alpha_S(\mu)}{2\pi}\right)^2\left[\bar{\mathcal{B}}(\chi, \mu) - \frac{1}{2}\bar{\mathcal{A}}^2(\chi, \mu)\right]\\
&+\left(\frac{\alpha_S(\mu)}{2\pi}\right)^3\left[\bar{\mathcal{C}}(\chi, \mu) - \bar{\mathcal{A}}(\chi, \mu)\bar{\mathcal{B}}(\chi, \mu)\right.\\
&\left.+\frac{1}{3}\bar{\mathcal{A}}^3(\chi, \mu)\right].
\end{aligned} \tag{14}$$

[4] We note that another resummation in the forward limit would be required to describe EEC over the full angular range.

[5] Note a misprint in Eq. (3.12) of Ref. [23] where an overall factor of $1/2$ appears erroneously.

Here $\left\{\frac{1}{H(\alpha_S(\mu))}\left[\frac{1}{\sigma_t}\widetilde{\Sigma}(\chi,\mu)\right]_{res.}\right\}_{f.o.}$ is the fixed-order expansion of the resummed result,

$$\begin{aligned}\frac{1}{H(\alpha_S(\mu))}\left[\frac{1}{\sigma_t}\widetilde{\Sigma}(\chi,\mu)\right]_{res.} &= 1+\frac{\alpha_S(\mu)}{2\pi}\bar{\mathcal{A}}_{res.}(\chi,\mu)\\ &+\left(\frac{\alpha_S(\mu)}{2\pi}\right)^2\bar{\mathcal{B}}_{res.}(\chi,\mu)\\ &+\left(\frac{\alpha_S(\mu)}{2\pi}\right)^3\bar{\mathcal{C}}_{res.}(\chi,\mu)\\ &+\mathcal{O}(\alpha_S^4).\end{aligned} \tag{15}$$

The expansion coefficients $\bar{\mathcal{A}}_{res.}$, $\bar{\mathcal{B}}_{res.}$ and $\bar{\mathcal{C}}_{res.}$ can be found in Ref. [23].

Notice that the function $H(\alpha_S)$ does not appear in Eq. (14) at all. In the log-R matching scheme such non-logarithmically enhanced contributions should not be exponentiated, instead these terms, as well as subdominant logarithmic contributions, are all implicit in the unsubtracted parts of the fixed-order coefficients $\bar{\mathcal{A}}$, $\bar{\mathcal{B}}$ and $\bar{\mathcal{C}}$ [41]. Thus the log-R matched prediction can be computed without the explicit knowledge of $H^{(n)}$.

Finally, we comment on our implementation of the unitarity constraint $\widetilde{\Sigma}(\pi,\mu)/\sigma_t = 1$. It can be shown that this constraint can be satisfied by modifying the resummation formula in Eq. (4) such that in the kinematical limit $y = 1$ the Sudakov form factor is unity. This may be achieved in several ways and here we choose a very simple solution and modify the resummation coefficients $\tilde{A}^{(n)}$ and $\tilde{B}^{(n)}$ according to

$$\begin{aligned}\tilde{A}^{(n)}(x_L) &\to \tilde{A}^{(n)}(y,x_L) = \tilde{A}^{(n)}(x_L)(1-y)^p,\\ \tilde{B}^{(n)}(x_L) &\to \tilde{B}^{(n)}(y,x_L) = \tilde{B}^{(n)}(x_L)(1-y)^p,\end{aligned} \tag{16}$$

where p is a positive number.[6] This modification is fully legitimate since it does not modify the logarithmic structure of the result and introduces only power-suppressed terms. In practice, we set $p = 1$ and quantify the impact of this modification by comparing the results to those obtained with $p = 2$.

2.3 Finite b-quark mass corrections

The theoretical prediction presented above was computed in massless QCD. However, the assumption of vanishing quark masses is not fully justified, especially at lower energies, where b-quark mass effects are relevant at the percent level [43]. In order to take b-quark mass corrections into account, we subtract the fraction of b-quark events, $r_b(Q)$ from the massless result and add back the corresponding massive contribution. Hence, we include mass effects directly at the level of matched distributions,

$$\begin{aligned}\frac{1}{\sigma_t}\frac{d\Sigma(\chi,Q)}{d\cos\chi} &= (1-r_b(Q))\left[\frac{1}{\sigma_t}\frac{d\Sigma(\chi,Q)}{d\cos\chi}\right]_{massless}\\ &+r_b(Q)\left[\frac{1}{\sigma_t}\frac{d\Sigma(\chi,Q)}{d\cos\chi}\right]^{NNLO^*}_{massive}.\end{aligned} \tag{17}$$

Here $\left[\frac{1}{\sigma_t}\frac{d\Sigma(\chi,Q)}{d\cos\chi}\right]_{massless}$ is the NNLO+NNLL matched distribution, computed in the log-R matching scheme in massless QCD as outlined above, while $\left[\frac{1}{\sigma_t}\frac{d\Sigma(\chi,Q)}{d\cos\chi}\right]^{NNLO^*}_{massive}$ is the fixed-order massive distribution. As the complete NNLO correction to this distribution is currently unknown, we model it by supplementing the massive NLO prediction of the parton level Monte Carlo generator `Zbb4` [44], with the NNLO coefficient of the massless fixed-order result.

We define the fraction of b-quark events as the ratio of the total b-quark production cross section divided by the total hadronic cross section,

$$r_b(Q) \equiv \frac{\sigma_{massive}(e^+e^-\to b\bar{b})}{\sigma_{massive}(e^+e^-\to \text{hadrons})}.$$

We evaluate the ratio of these cross sections at NNLO accuracy ($\mathcal{O}(\alpha_S^2)$ in the strong coupling) including the exact b-quark mass corrections at $\mathcal{O}(\alpha_S)$ and the leading mass terms up to $(m_b^2/Q^2)^2$ at $\mathcal{O}(\alpha_S^2)$ [45]. We note that the electroweak coupling factors do not cancel in this ratio and the summation over quark flavours has to be carried out explicitly when computing $\sigma_{massive}(e^+e^-\to \text{hadrons})$.

Distributions for $\left[\frac{1}{\sigma_t}\frac{d\Sigma(\chi,Q)}{d\cos\chi}\right]_{massive}$ were generated for each of the considered energies using a pole b-quark mass of $m_b = 4.75\,\text{GeV}$, which is consistent with world average estimations of pole mass $4.78 \pm 0.06\,\text{GeV}$ [46].

In order to assess the uncertainty associated to the modelling of b-quark mass corrections, we have investigated two alternative approaches for including them in our predictions. In approach A Eq. (17) is modified to

$$\begin{aligned}\frac{1}{\sigma_t}\frac{d\Sigma(\chi,Q)}{d\cos\chi} &= \left[\frac{1}{\sigma_t}\frac{d\Sigma(\chi,Q)}{d\cos\chi}\right]_{massless}\\ &+r_b(Q)\left[\frac{1}{\sigma_t}\frac{d\Sigma(\chi,Q)}{d\cos\chi}\right]^{NLO}_{massive}\\ &-r_b(Q)\left[\frac{1}{\sigma_t}\frac{d\Sigma(\chi,Q)}{d\cos\chi}\right]^{NLO}_{massless},\end{aligned}$$

i.e., we simply subtract the massless fixed-order NLO prediction multiplied by the fraction $r_b(Q)$ of b-quark events and add back the corresponding massive NLO distribution. Approach B is defined in a way very similar to our baseline, Eq. (17), but we do not include any NNLO corrections to the massive distribution,

[6] A modification similar in spirit was employed in Ref. [42] although in the context of matching the fixed-order and resummed predictions for transverse observables in Higgs hadroproduction.

Table 1 Data used in the extraction procedure. The average of $\sqrt{s}$ is given in the brackets

Experiment	$\sqrt{s}$, GeV, data	$\sqrt{s}$, GeV, MC	Events
SLD [47]	91.2 (91.2)	91.2	60,000
OPAL [50]	91.2 (91.2)	91.2	336,247
OPAL [51]	91.2 (91.2)	91.2	128,032
L3 [48]	91.2 (91.2)	91.2	169,700
DELPHI [49]	91.2 (91.2)	91.2	120,600
TOPAZ [52]	59.0−60.0 (59.5)	59.5	540
TOPAZ [52]	52.0−55.0 (53.3)	53.3	745
TASSO [53]	38.4−46.8 (43.5)	43.5	6434
TASSO [53]	32.0−35.2 (34.0)	34.0	52,118
PLUTO [58]	34.6 (34.6)	34.0	6964
JADE [54]	29.0−36.0 (34.0)	34.0	12,719
CELLO [57]	34.0 (34.0)	34.0	2600
MARKII [56]	29.0 (29.0)	29.0	5024
MARKII [56]	29.0 (29.0)	29.0	13,829
MAC [55]	29.0 (29.0)	29.0	65,000
TASSO [53]	21.0−23.0 (22.0)	22.0	1913
JADE [54]	22.0 (22.0)	22.0	1399
CELLO [57]	22.0 (22.0)	22.0	2000
TASSO [53]	12.4−14.4 (14.0)	14.0	2704
JADE [54]	14.0 (14.0)	14.0	2112

$$\frac{1}{\sigma_t}\frac{\mathrm{d}\Sigma(\chi,Q)}{\mathrm{d}\cos\chi} = (1-r_b(Q))\left[\frac{1}{\sigma_t}\frac{\mathrm{d}\Sigma(\chi,Q)}{\mathrm{d}\cos\chi}\right]_{\text{massless}} + r_b(Q)\left[\frac{1}{\sigma_t}\frac{\mathrm{d}\Sigma(\chi,Q)}{\mathrm{d}\cos\chi}\right]^{NLO}_{\text{massive}}.$$

Hence, $\left[\frac{1}{\sigma_t}\frac{\mathrm{d}\Sigma(\chi,Q)}{\mathrm{d}\cos\chi}\right]^{NLO}_{\text{massive}}$ is simply the prediction obtained with `Zbb4`.

3 Extraction procedure

To extract the strong coupling the predictions described above were confronted with the available data sets. Namely, the data obtained in SLD [47], L3 [48], DELPHI [49], OPAL [50,51], TOPAZ [52], TASSO [53], JADE [54], MAC [55], MARKII [56], CELLO [57] and PLUTO [58] experiments were included. The information on used data is summarised in Tab. 1.

The criteria to include the data were high precision of differential distributions obtained with charged and neutral final state particles in the full χ range, presence of corrections for detector effects, correction for initial state photon radiation and sufficient amount of supplementary information. Therefore, data sets without supplementary information [59], with large uncertainties [60], superseded datasets [61,62] and measurements unfolded only to charged particles in the final state [63] are not included in the analysis.

The data sets selected for the extraction procedure have high precision and the measurements from different experiments performed at close energy points are consistent.[7] This justifies their use in the extraction procedure in a wide centre-of-mass energy interval, similarly to studies of thrust [43] and C parameter [64] and allows us to target the highest precision of α_S determination with available theoretical predictions.

3.1 Monte Carlo generation setup

In a previous study [23] the non-perturbative effects for the EEC distribution were modelled with an analytic approach. In this paper the non-perturbative effects in the $e^+e^- \to hadrons$ process are modelled using state-of-the-art particle-level Monte Carlo (MC) generators. The non-perturbative corrections of the energy–energy correlation distributions were extracted as ratios of energy–energy correlation distributions at hadron and parton level in the simulated samples.

In this study the MC generators `SHERPA2.2.4` [65][8] and `Herwig7.1.1`, [66–68] were used.

The $e^+e^- \to hadrons$ MC samples were generated at centre-of-mass energies $\sqrt{s} = 14.0$, 22.0, 29.0, 34.0, 43.5, 53.3, 59.5 and 91.2 GeV. In all cases, the simulation of initial state radiation was disabled and generator settings were defaults if the opposite is not stated explicitly. The value of the strong coupling used for the hard process was set to $\alpha_S(M_Z) = 0.1181$ [46].

The `SHERPA2.2.4` samples were generated with the MENLOPS method using the matrix element generators `AMEGIC` [69], `COMIX` [70] and the `GoSam` [71] one-loop library to produce matrix elements for $e^+e^- \to Z/\gamma \to$ 2, 3, 4, 5 partons processes. The 2−parton final state processes had NLO accuracy in perturbative QCD. The QCD matrix elements were calculated assuming massive b-quarks. The merging parameter Y_{cut} was set to $10^{-2.75} \simeq 1.778 \times 10^{-3}$.

To test the fragmentation and hadronization model dependence, the events generated with `SHERPA2.2.4` were hadronized using the Lund string fragmentation model [72] or the cluster fragmentation model [73]. The first setup is labelled below as S^L and the second as S^C.

To assure proper fragmentation of heavy quarks and heavy hadron decays the cluster fragmentation model was adjusted. The value of `SPLIT_LEADEXPONENT` parameter was set to 1.0, the parameter `M_DIQUARK_OFFSET` was set to 0.55,

[7] Some observed differences between the measurements performed at $\sqrt{s} = 91.2$ GeV are not statistically significant once the systematical uncertainties and correlations are taken into account.

[8] Partially updated to version 2.2.5.

the production of charm and beauty baryons was enhanced by factors 0.8 and 1.7.

For the cross-check of SHERPA2.2.4 samples, the Herwig7.1.1 generator was used. The Herwig7.1.1 samples were generated with improved unitarized merging [74] using the MadGraph5 [75] matrix element generator and the GoSam [71] one-loop library to produce matrix elements of the $e^+e^- \to Z/\gamma \to 2, 3, 4, 5$ partons processes. The 2−parton final state processes again had NLO accuracy in perturbative QCD and the matrix elements were calculated assuming massive b-quarks. The merging parameter was set to $\sqrt{s} \times 10^{-1.25} \simeq \sqrt{s} \times 5.623 \times 10^{-2}$. For the modelling of the hadronization process the default implementation of the cluster fragmentation model [76] was used. To improve the modelling of beauty production at the lowest energies, the b-quark nominal mass was changed from the default value of 5.3 GeV to 5.1 GeV. This setup is labelled below as H^M.

3.2 Estimation of hadronization effects from MC models

Estimation of hadronization corrections is an integral part of comparing the parton-level QCD predictions to the data measured on hadron (particle) level. Despite the fact that under certain conditions the local parton-hadron duality leads to close values of quantities on parton and hadron level, the difference between them is not negligible and should be taken into account in precise analyses. One way to do so is to apply correction factors estimated from MC simulations to the perturbative QCD prediction. The factors, called hadronization corrections H/P, are defined as ratios of the corresponding quantities at parton level to the same quantities at hadron level at every point of the considered distribution.

To obtain the EEC distributions, the generated MC samples were processed in the same way as data (see e.g. Ref. [50]), using partons before hadronization for parton-level calculations and undecayed/stable particles for hadron-level calculations. For the parton-level calculations the parton energies were used as provided by the MC generators.

The predictions obtained with all setups describe the data well for all ranges of χ with the exception of the regions near $\chi = 0°$ and $\chi = 90°$, for all values of $\sqrt{s}$. For $\sqrt{s} <$ 29 GeV the H^M setup is sensitive to the b-quark mass and the corresponding predictions are not reliable.

However, to assure an even better description of data, a reweighting procedure was applied to the simulated samples. The samples were reweighted at hadron level on an event-by-event basis to describe the data and the corresponding event weights were propagated to the parton level. The resulting distributions are shown in Fig. 1 for the SHERPA2.2.4 setups and in Fig. 2 for the Herwig7.1.1 setup.

As the SHERPA2.2.4 setups give the most stable and physically reliable predictions these are used in the analysis for reference hadronization corrections (S^L) and for system-

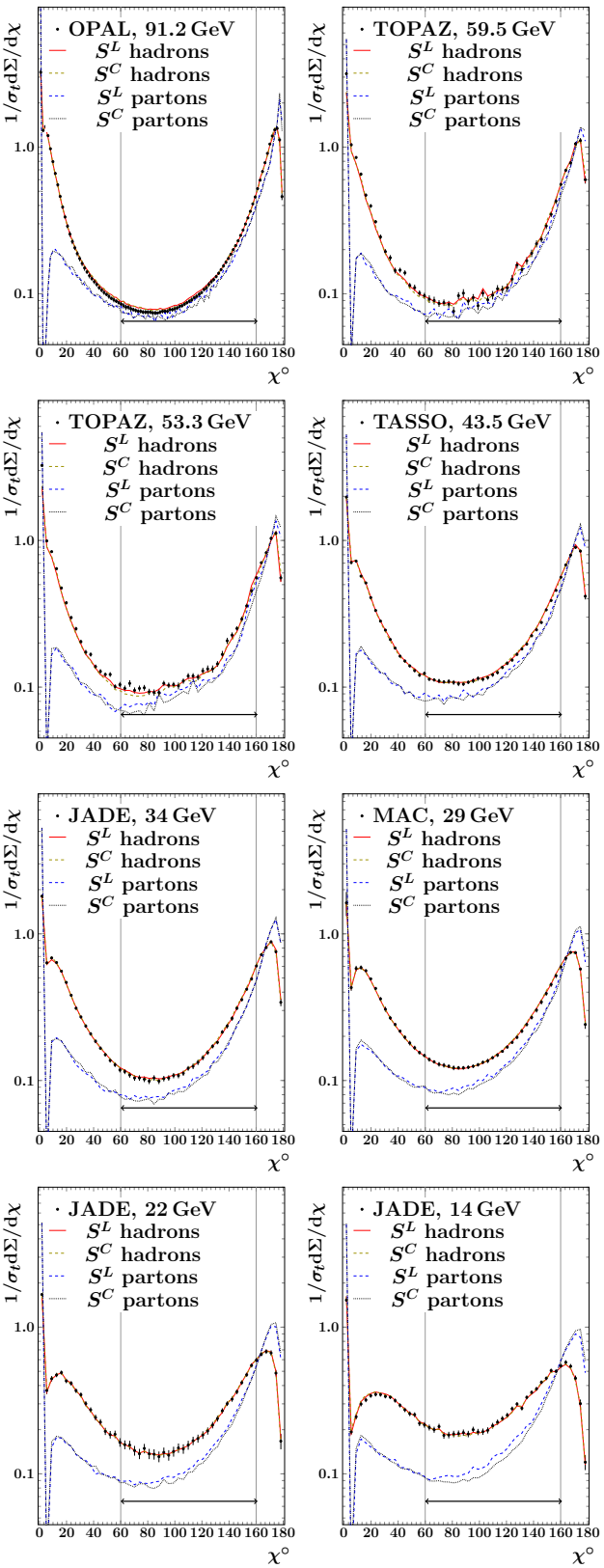

Fig. 1 Data and Monte Carlo predictions obtained with the S^L and S^C setups at parton and hadron level. Reweighting was applied

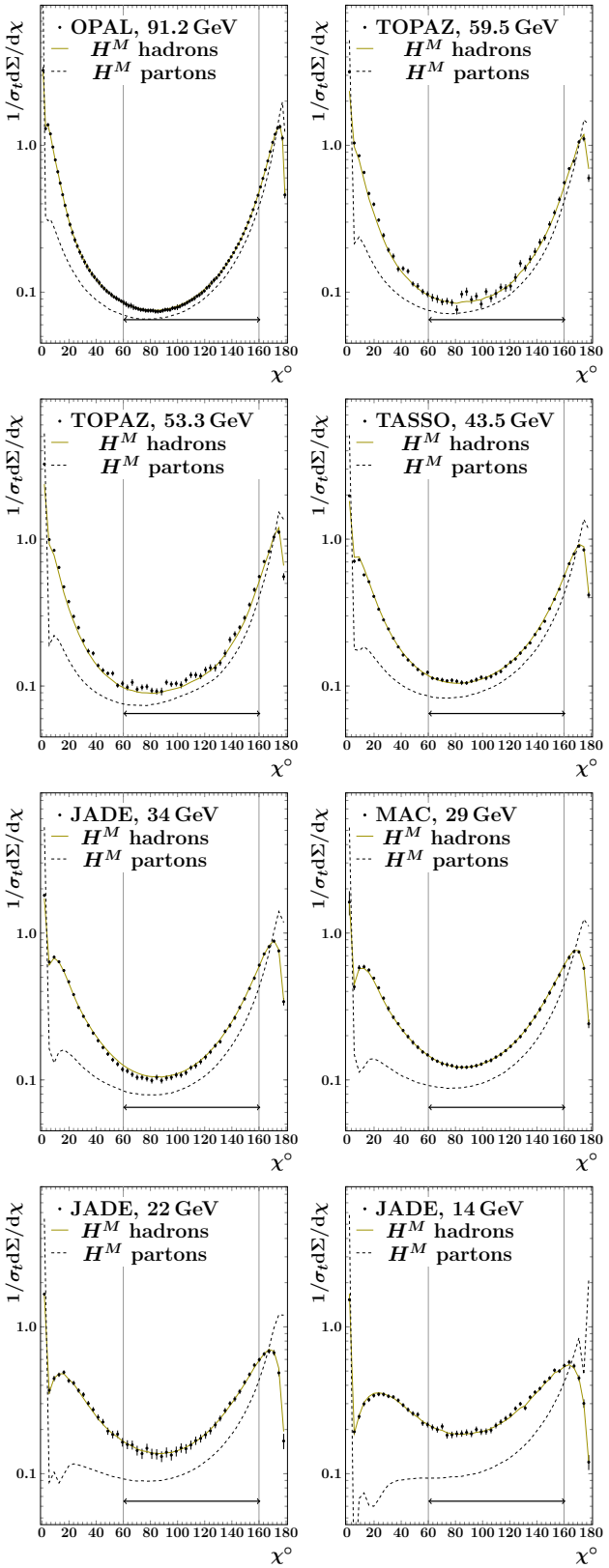

Fig. 2 Data and Monte Carlo predictions obtained with the H^M setup at parton and hadron level. Reweighting was applied

atic studies (S^C). The corresponding hadronization corrections together with parametrizations are shown in Fig. 3 for reweighted samples.

3.3 Estimation of statistical correlations between measurements from MC models

To perform an accurate extraction procedure, the available data and uncertainties were examined and for every measured set of data a covariance matrix was built. The procedure consisted of multiple steps.

In the first step the systematic uncertainties were recalculated and separated from statistical uncertainties when this was possible. For the measurements with the uncertainties rounded to one significant digit [50,53,54] the uncertainties were expanded assuming maximal uncertainty before rounding. The measurements of TASSO [53] were converted from the $d\Sigma/d\cos\chi$ form to $d\Sigma/d\chi$ using values of $\cos\chi$ on the bin edges.

For the data from TOPAZ [52] the systematic uncertainty was calculated from an estimated relative systematic uncertainty of $\pm 4\%$ [52].

Taking into account the uncertainties of α_S extraction analysis [58] the same was done for PLUTO [58] data. The systematic uncertainty estimation of $\pm 5\%$ for TASSO [53] is based on the upper limit of 10% for the total uncertainty mentioned in the paper [53]. The systematic uncertainties from DELPHI [49] and SLD [47] were used as provided in the original papers.

For all remaining data sets the published combined uncertainty was treated as statistical.

The measurements of Σ are provided in the original publications without correlations between the individual points. The correlation matrix was estimated from the Monte Carlo samples in terms of Fisher correlation coefficients [77,78]. Some of the obtained correlation matrices are shown in Fig. 4.

The obtained correlation coefficients are sizeable, up to 0.5 for the closest points, which highlights the importance of properly taking into account the correlations between measured points in the fits. The obtained correlation matrix together with statistical uncertainties was used to build a statistical covariance matrix for every data set.

To construct the systematic covariance matrix, the systematic uncertainties from the original publications were used with an assumption that these are positively correlated with correlation coefficient $\rho = 0.5$ between closest points. The correlations between the uncertainties of data from different experiments or different beam energies were neglected. The final covariance matrix used in the fit for every data set was a sum of statistical and systematic covariance matrices.

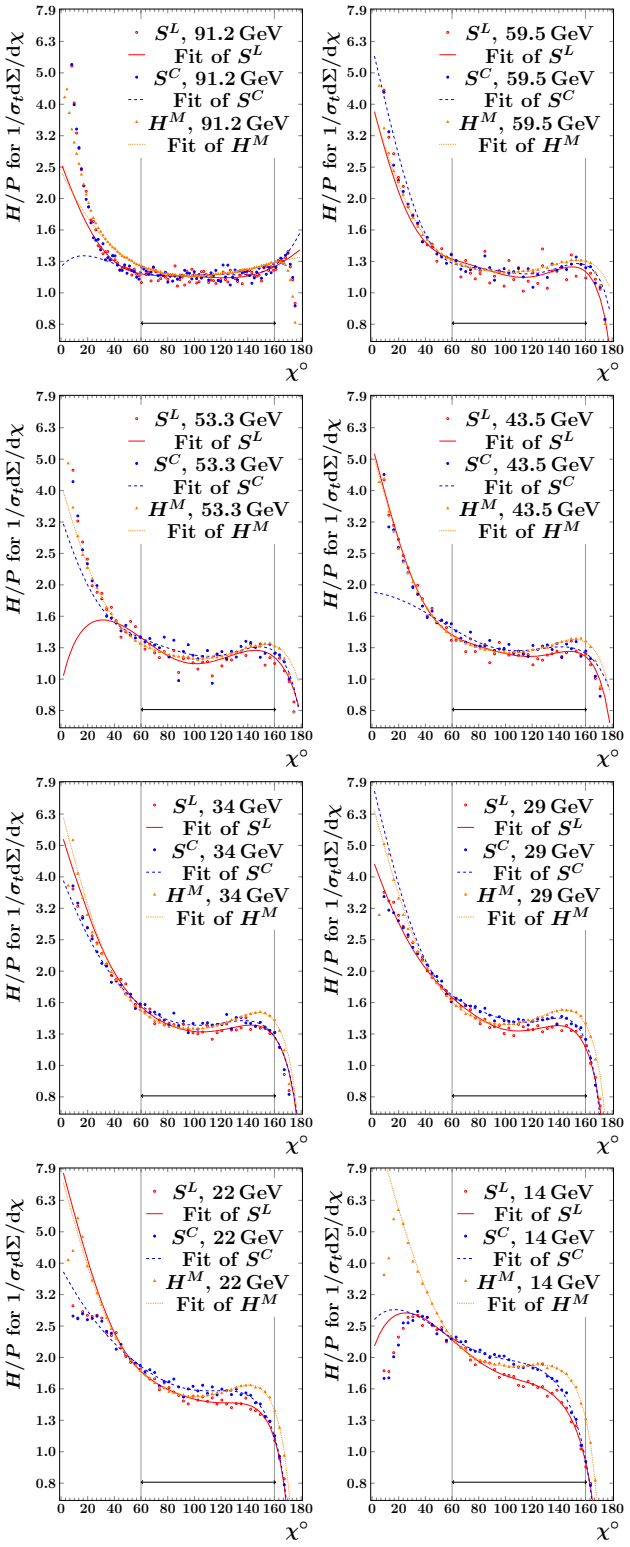

Fig. 3 Hadronization corrections obtained with different setups of Monte Carlo event simulations for every energy point and corresponding parametrizations. Event-by-event reweighting was applied. The used fit range is indicated with a thick line

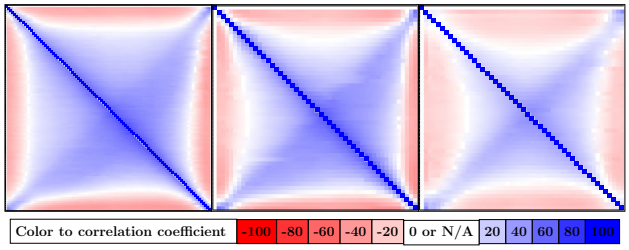

Fig. 4 A graphical representation of statistical correlation matrices for $\Sigma(\chi)$ obtained from Monte Carlo simulated events with the S^L setup for OPAL [51] data at $\sqrt{s} = 91.2\,\mathrm{GeV}$ (left), TOPAZ [52] data at $\sqrt{s} = 53.3\,\mathrm{GeV}$ (centre), and JADE [54] data at $\sqrt{s} = 22\,\mathrm{GeV}$ (right). The bottom left corner for each figure corresponds to $\chi = 0°$ and the bottom right to $\chi = 180°$

3.4 Fit procedure and estimation of uncertainties

The strong coupling extraction procedure is based on the comparison of data to the perturbative QCD prediction combined with non-perturbative (hadronization) corrections. The perturbative part of the predictions was calculated in every bin as described in previous sections. To tame the statistical fluctuations present in the obtained binned hadronization correction distributions, these were parametrized with analytic functions, expressed as a sum of polynomials of $\chi - 90°$. The value of the fitted function at the bin centre was used as the correction factor.

To find the optimal value of α_S, the `MINUIT2` [79,80] program was used to minimize

$$\chi^2(\alpha_S) = \sum_{\text{data sets}} \chi^2(\alpha_S)_{\text{data set}},$$

where the $\chi^2(\alpha_S)$ value was calculated for each data set as

$$\chi^2(\alpha_S) = (\boldsymbol{D} - \boldsymbol{P}(\alpha_S)) V^{-1} (\boldsymbol{D} - \boldsymbol{P}(\alpha_S))^T,$$

with $\boldsymbol{D}$ standing for the vector of data points, $\boldsymbol{P}(\alpha_S)$ for the vector of calculated predictions and V for the covariance matrix for $\boldsymbol{D}$. The default scale used in the fit procedure was $\mu = Q = \sqrt{s}$.

The fit ranges were chosen to avoid regions where resummed predictions or hadronization correction calculations are not reliable. The selected fit ranges were $117°-165°$, $60°-165°$ and $60°-160°$. The uncertainty on the fit result was estimated with the $\chi^2 + 1$ criterion as implemented in the `MINUIT2` program. The results of the fits are given in Tab. 2 for each fit range. In order to assess the impact of the NNLO corrections, in Tab. 2 we also present the results obtained using NLO+NNLL predictions. The NNLO corrections affect the fit in a moderate but non-negligible way. The obtained values of χ^2 divided by the number of degrees of freedom in the fit are of order unity for all cases. The corresponding distributions obtained from the fits for different $\sqrt{s}$ points are shown in Figs. 5, 6, 7 and 8.

Table 2 Results of the fits of the matched predictions at NLO+NNLL and NNLO+NNLL accuracy to experimental data. The given uncertainty is fit uncertainty scaled by $\sqrt{\chi^2/ndof}$

Fit range, °	NLO+NNLL	NNLO+NNLL
Hadronization	$\chi^2/ndof$	$\chi^2/ndof$
117°−165°	0.12042 ± 0.00025	0.11760 ± 0.00020
S^L	$765/298 = 2.57$	$513/298 = 1.72$
60°−165°	0.12134 ± 0.00022	0.11746 ± 0.00018
S^L	$1720/664 = 2.59$	$1211/664 = 1.82$
60°−160°	0.12200 ± 0.00023	0.11750 ± 0.00018
S^L	$1417/623 = 2.27$	$1022/623 = 1.64$
117°−165°	0.11796 ± 0.00022	0.11521 ± 0.00017
S^C	$631/298 = 2.12$	$395/298 = 1.32$
60°−165°	0.11900 ± 0.00021	0.11530 ± 0.00015
S^C	$1557/664 = 2.34$	$951/664 = 1.43$
60°−160°	0.11973 ± 0.00022	0.11545 ± 0.00016
S^C	$1321/623 = 2.12$	$845/623 = 1.36$
117°−165°	0.11272 ± 0.00037	0.11044 ± 0.00029
H^M	$1842/298 = 6.18$	$1201/298 = 4.03$
60°−165°	0.11472 ± 0.00033	0.11180 ± 0.00023
H^M	$3845/664 = 5.79$	$2203/664 = 3.32$
60°−160°	0.11634 ± 0.00033	0.11281 ± 0.00023
H^M	$3091/623 = 4.96$	$1738/623 = 2.79$
117°−165°	0.12154 ± 0.00045	0.11781 ± 0.00037
$An.^{DMW}$	$730/295 = 2.48$	$558/295 = 1.89$
60°−165°	0.13555 ± 0.00052	0.12937 ± 0.00039
$An.^{DMW}$	$7525/661 = 11.38$	$4896/661 = 7.41$
60°−160°	0.13606 ± 0.00061	0.12950 ± 0.00044
$An.^{DMW}$	$7364/620 = 11.88$	$4827/620 = 7.78$

The systematic uncertainties of the obtained results were estimated with procedures used in previous studies [81]. To estimate the bias of the obtained result caused by the absence of higher-order terms in the perturbative predictions, the renormalization scale variation procedure was performed. In this procedure the fits were repeated, with variation of the renormalization scale in the range between $x_R = 1/2$ and $x_R = 2$.

The bias of hadronization model selection is studied using the S^L and S^C setups of hadronization corrections, see results in Fig. 9. The bias related to the ambiguity of resummation scale choice was estimated by varying x_L in the range between $x_L = 1/2$ and $x_L = 2$. To estimate the bias related to the ambiguity of our prescription implementing the unitarity constraint in the resummed calculation (see Eq. (16)), two values of p were used: $p = 1$ and $p = 2$. The difference between results obtained with two options is negligible. In all cases above the sizes of the biases were estimated numerically as half of the difference between the maximal and minimal α_S value obtained in the corresponding set of fits. To estimate the potential bias of the result caused by imperfections of specific hadronization model and parton shower model, the fits were repeated with hadronization corrections obtained with all setups described in previous subsections. The numerical value of the bias was obtained as half of the difference between the α_S values obtained using non-

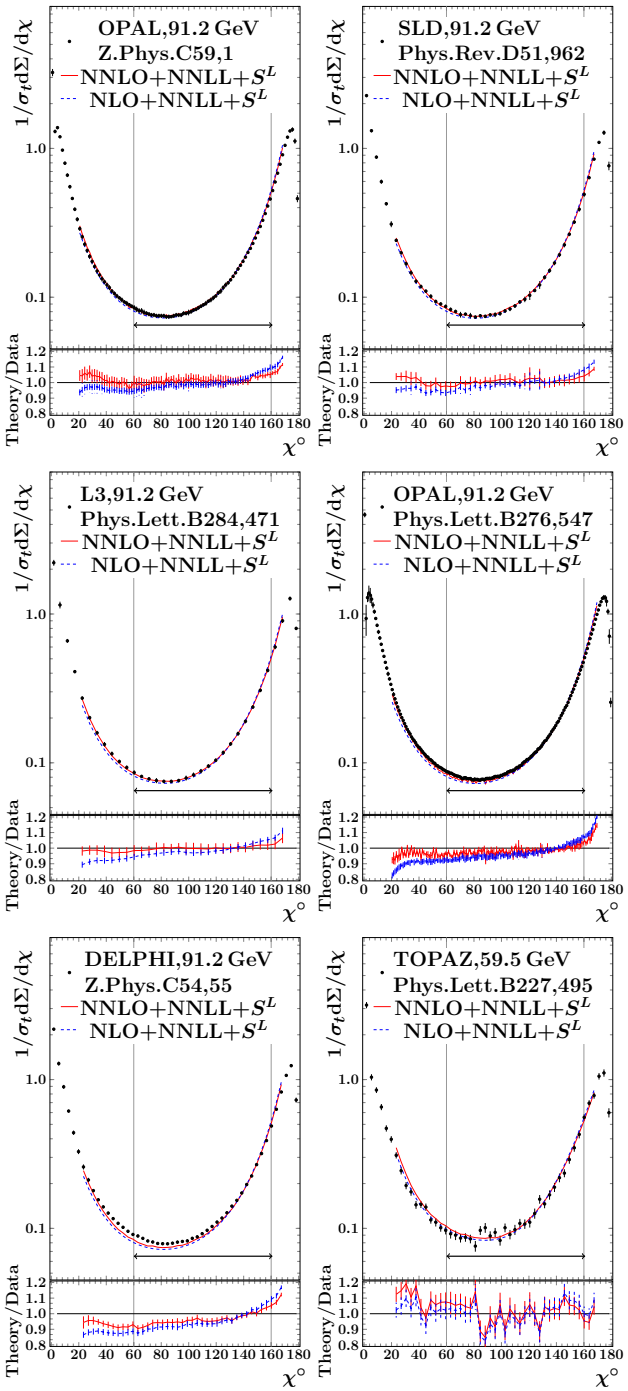

Fig. 5 Fits of theory predictions to the data at $\sqrt{s} = 59.5 - 91.2$ GeV. The used fit range is shown with thick line. For the ratio plot only the uncertainties of the data are taken into account

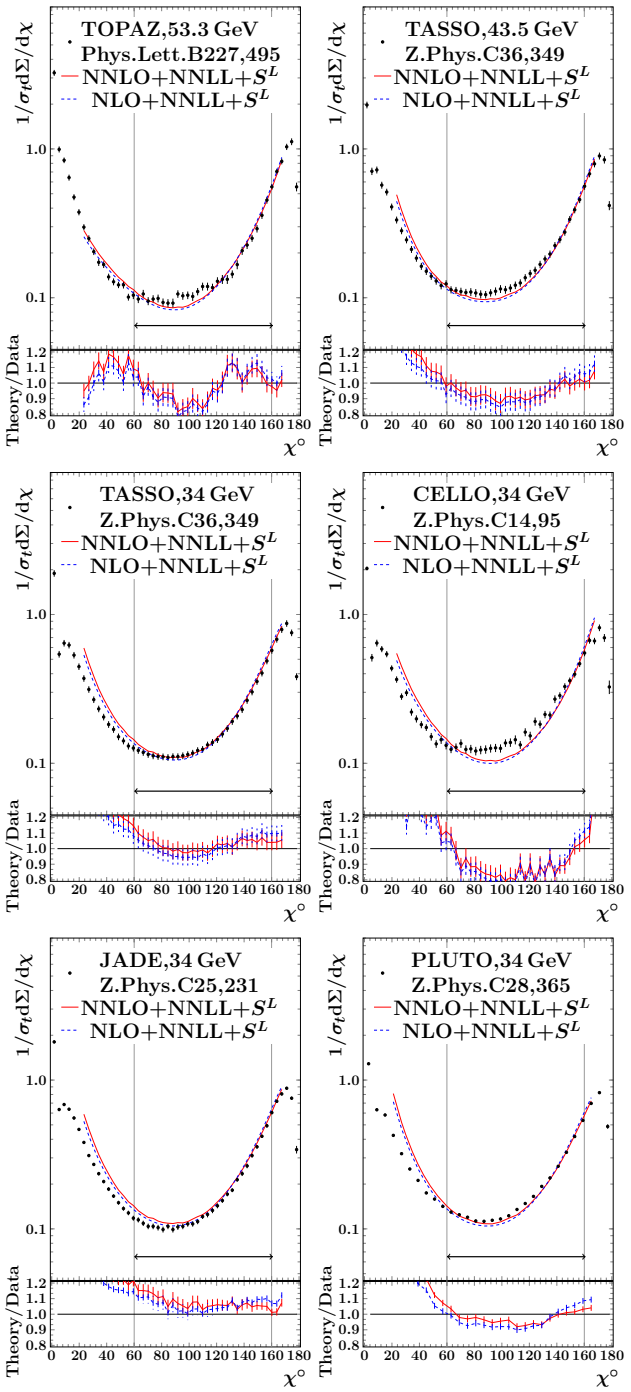

Fig. 6 Fits of theory predictions to the data for $\sqrt{s} = 34 - 53.3$ GeV. The used fit range is shown with thick line. For the ratio plot only the uncertainties of the data are taken into account

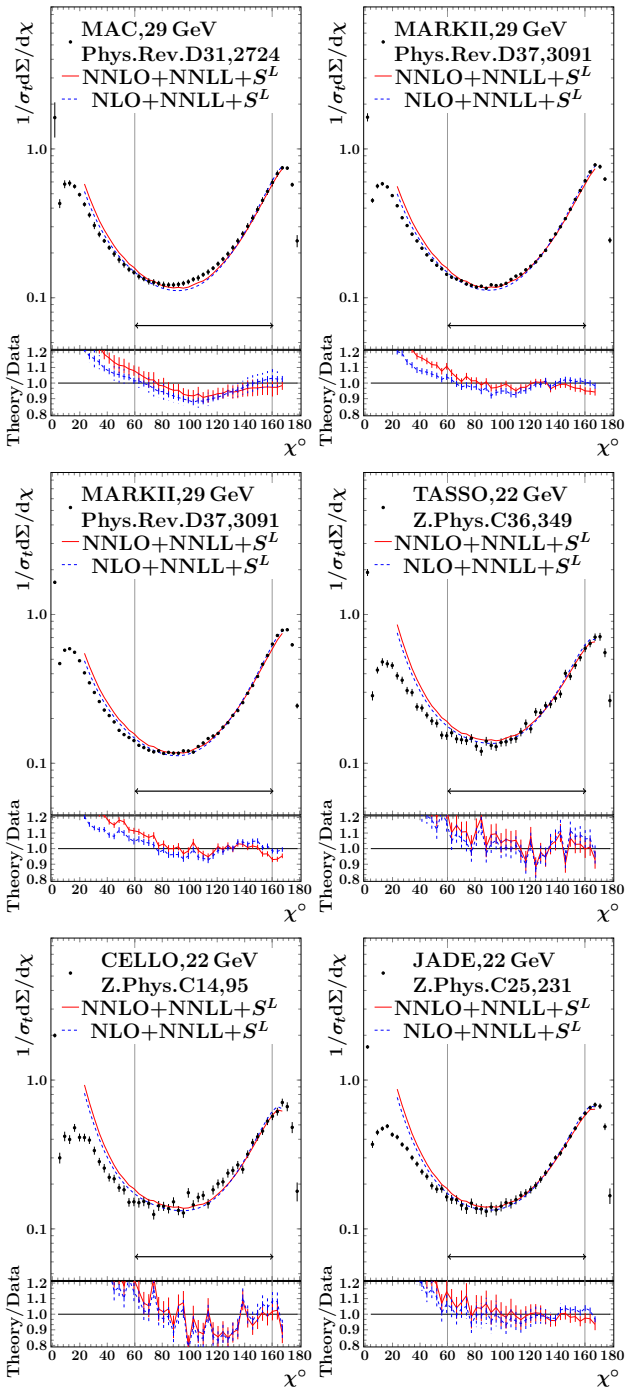

Fig. 7 Fits of theory predictions to the data for $\sqrt{s} = 22 - 29$ GeV. The used fit range is shown with thick line. For the ratio plot only the uncertainties of the data are taken into account

perturbative corrections from Lund and cluster hadronization models implemented in SHERPA2.2.4. From Fig. 9 it is seen that the estimated biases are relatively independent and, therefore combined in the final result as such.

Besides the estimations, several cross-checks of the obtained results were performed. First, the datasets were grouped according to their energies and fitted separately for each energy. The results are shown in Fig. 10. There is no visible trend for the fitted value of α_S with energy in the S^L and S^C setups. For the H^M setup, the results of the fits are not reliable below $\sqrt{s} < 29$ GeV due to the sensitivity of this setup to the b-quark mass. In addition to the MC hadroniza-

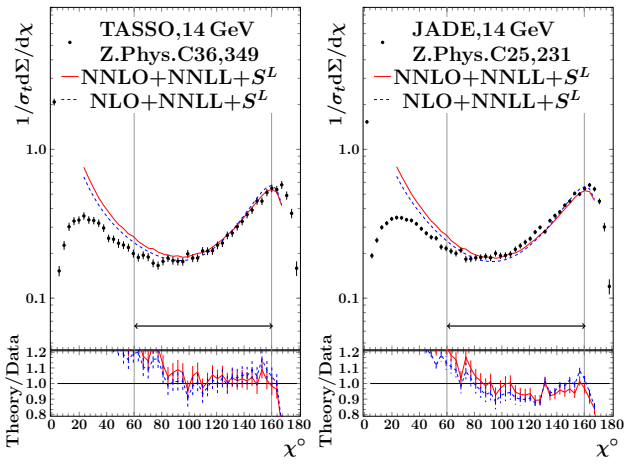

Fig. 8 Fits of theory predictions to the data for $\sqrt{s} = 14$ GeV. The used fit range is shown with thick line. For the ratio plot only the uncertainties of the data are taken into account

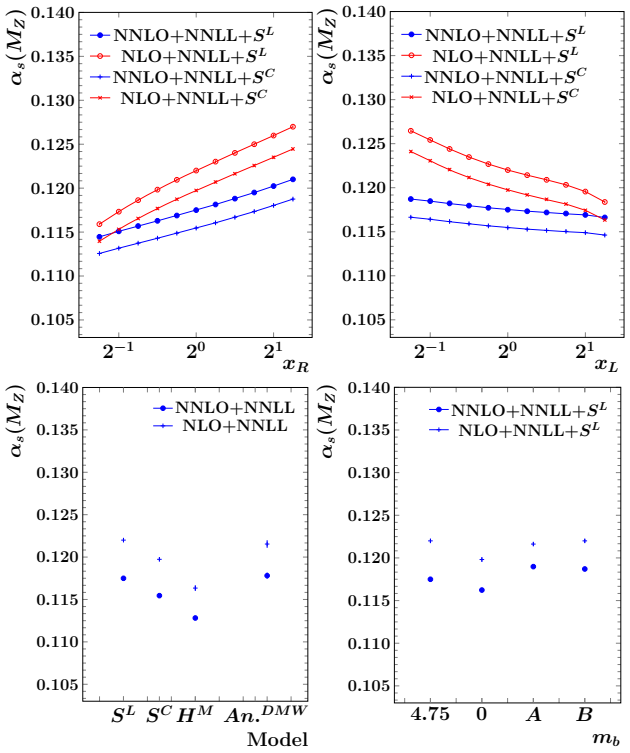

Fig. 9 Dependence of fit results on the renormalization scale (upper left), resummation scale (upper right), non-perturbative simulation model (bottom left) choice and b mass corrections (bottom right). The fit range for S^L, S^C and H^M setups is 60°−160°. The fit range for the $An.^{DMW}$ setup is 117°−165°

tion models the fits were also performed with the analytic hadronization model of Dokshitzer, Marchesini and Webber (DMW) [82]. In this setup, non-perturbative effects in EEC were accounted for by multiplying the Sudakov form factor by a correction of the form

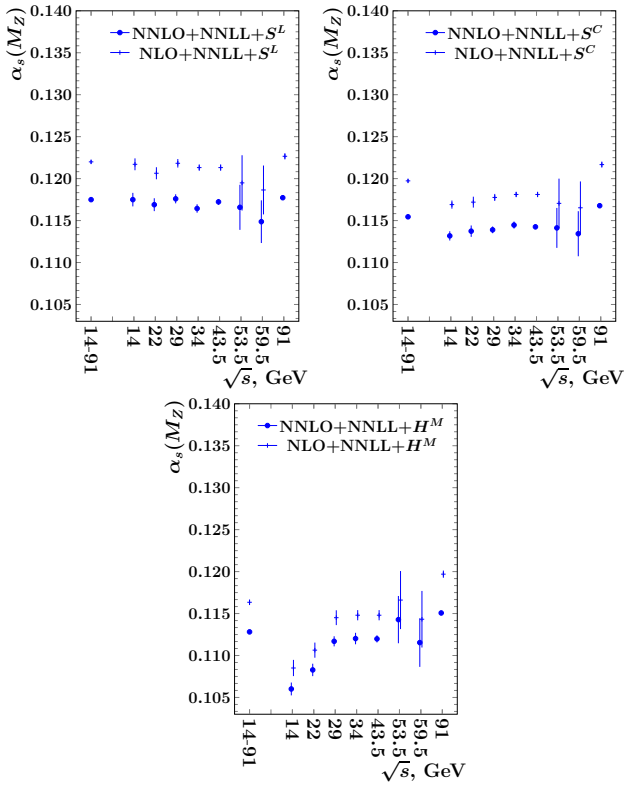

Fig. 10 Dependence of fit results on the used data sets. The fit range for S^L, S^C and H^M setups is 60°−160°

$$S_{\mathrm{NP}} = e^{-\frac{1}{2}a_1 b^2}(1 - 2a_2 b).$$

Here a_1 and a_2 are non-perturbative parameters that can be related in the dispersive approach to certain moments $\bar{\alpha}_{q,p}$ of the strong coupling α_S [82]. These moments are the fit parameters of the analytic model. The results obtained from the fits with this setup are listed in Tab. 2. They show a high degree of dependence on the selected fit range, but are close to results obtained with the Monte Carlo based hadronization corrections in the range 117°−165°, see Tab. 2. Hence we conclude that away from the back-to-back region, the analytic model cannot fully account for hadronization effects.

4 Results and discussions

In this paper we presented the first combined analysis and extraction of α_S at NNLO+NNLL precision from energy–energy correlation in electron-positron annihilation. Moreover, our analysis is the first extraction of the strong coupling based on Monte Carlo hadronization corrections obtained from NLO Monte Carlo setups at NNLO+NNLL precision. For the central value of the final result we quote the results obtained from the fits with the S^L hadronization model in the

range $60°-160°$ with uncertainties and estimations of biases obtained as described above.

At NNLO+NNLL accuracy we obtain the best fit value of

$$\alpha_S(M_Z) = 0.11750 \pm 0.00018(exp.) \pm 0.00102(hadr.) \pm 0.00257(ren.) \pm 0.00078(res.).$$

In order to appreciate the impact of NNLO corrections, we also quote the result of the fit at NLO+NNLL accuracy

$$\alpha_S(M_Z) = 0.12200 \pm 0.00023(exp.) \pm 0.00113(hadr.) \pm 0.00433(ren.) \pm 0.00293(res.).$$

We see that the inclusion of the NNLO corrections has a moderate but non-negligible effect on the extracted value of α_S.

It has been explicitly checked that there are no correlations between estimated biases, therefore, the combined values with combined estimations of bias at NNLO+NNLL accuracy are:

$$\alpha_S(M_Z) = 0.11750 \pm 0.00287(comb.)$$

while in comparison, for NLO+NNLL accuracy we obtain:

$$\alpha_S(M_Z) = 0.12200 \pm 0.00535(comb.).$$

The value obtained from the analysis in NNLO+NNLL approximation is in agreement with the world average as of 2017 [83], however it is visibly lower than the results from measurements performed for other e^+e^- observables using NNLO perturbative QCD predictions and MC hadronization models [83]. The estimated uncertainties are dominated by the uncertainty on the theoretical predictions. The results obtained in this study can be compared to those described in the original publications with NLO+NLL precision as well as the results obtained with analytic hadronization model in the sister paper [23].

Acknowledgements We are grateful to Simon Plätzer and Ludovic Scyboz for fruitful discussions about the calculation of NLO predictions with `Herwig7.1.1` and `GoSam`, to Pier Monni for stimulating discussions on resummation of event shapes and to Carlo Oleari for providing us the `Zbb4` code. ZT was supported by the ÚNKP-17-3 New National Excellence Program of the Ministry of Human Capacities of Hungary. AK acknowledges financial support from the Premium Postdoctoral Fellowship program of the Hungarian Academy of Sciences. This work was supported by Grant K 125105 of the National Research, Development and Innovation Fund in Hungary.

References

1. H. Fritzsch, M. Gell-Mann, H. Leutwyler, Advantages of the color octet gluon picture. Phys. Lett. B **47**, 365 (1973)
2. D.J. Gross, F. Wilczek, Ultraviolet behavior of nonabelian gauge theories. Phys. Rev. Lett. **30**, 1343 (1973)
3. H.D. Politzer, Reliable perturbative results for strong interactions? Phys. Rev. Lett. **30**, 1346 (1973)
4. D.J. Gross, F. Wilczek, Asymptotically free gauge theories. 1. Phys. Rev. D **8**, 3633 (1973)
5. S. Kluth, Tests of quantum chromo dynamics at e^+e^- colliders. Rept. Prog. Phys. **69**, 1771 (2006). arXiv:hep-ex/0603011
6. G. Dissertori, The determination of the strong coupling constant. Adv. Ser. Direct. High Energy Phys. **26**, 113 (2016). arXiv:1506.05407
7. A. Gehrmann-De Ridder et al., NNLO corrections to event shapes in e^+e^- annihilation. JHEP **12**, 094 (2007). arXiv:0711.4711
8. S. Weinzierl, Event shapes and jet rates in electron–positron annihilation at NNLO. JHEP **06**, 041 (2009). arXiv:0904.1077
9. V. Del Duca et al., Jet production in the CoLoRFulNNLO method: event shapes in electron–positron collisions. Phys. Rev. D **94**, 074019 (2016). arXiv:1606.03453
10. V. Del Duca et al., Three-jet production in electron–positron collisions at next-to-next-to-leading order accuracy. Phys. Rev. Lett. **117**, 152004 (2016). arXiv:1603.08927
11. D. de Florian, M. Grazzini, The back-to-back region in e^+e^- energy–energy correlation. Nucl. Phys. B **704**, 387 (2005). arXiv:hep-ph/0407241
12. T. Becher, M.D. Schwartz, A precise determination of α_s from LEP thrust data using effective field theory. JHEP **07**, 034 (2008). arXiv:0803.0342
13. Yang-Ting Chien, M.D. Schwartz, Resummation of heavy jet mass and comparison to LEP data. JHEP **1008**, 058 (2010). arXiv:1005.1644
14. P.F. Monni, T. Gehrmann, G. Luisoni, Two-loop soft corrections and resummation of the thrust distribution in the dijet region. JHEP **08**, 010 (2011). arXiv:1105.4560
15. S. Alioli et al., Combining higher-order resummation with multiple NLO calculations and parton showers in GENEVA. JHEP **09**, 120 (2013). arXiv:1211.7049
16. T. Becher, G. Bell, NNLL resummation for jet broadening. JHEP **1211**, 126 (2012). arXiv:1210.0580
17. A. Banfi et al., A general method for the resummation of event-shape distributions in e^+e^- annihilation. JHEP **1505**, 102 (2015). arXiv:1412.2126
18. A. Hoang et al., C-parameter distribution at $\mathrm{N^3LL'}$ including power corrections. Phys. Rev. D **91**, 094017 (2015). arXiv:1411.6633
19. R. Abbate et al., Thrust at N^3LL with power corrections and a precision global fit for $\alpha_S(M_Z)$. Phys. Rev. D **83**, 074021 (2011). arXiv:1006.3080
20. T. Gehrmann, G. Luisoni, H. Stenzel, Matching NLLA + NNLO for event shape distributions. Phys. Lett. B **664**, 265 (2008). arXiv:0803.0695
21. L.J. Dixon et al., The energy–energy correlation at next-to-leading order in QCD, analytically. (2018). arXiv:1801.03219
22. C. Basham et al., Energy correlations in electron–positron annihilation: testing QCD. Phys. Rev. Lett. **41**, 1585 (1978)
23. Z. Tulipánt, A. Kardos, G. Somogyi, Energy–energy correlation in electron positron annihilation at NNLL + NNLO accuracy. Eur. Phys. J. C **77**, 749 (2017). arXiv:1708.04093
24. D.G. Richards et al., Energy–energy correlations to second order in quantum chromodynamics. Nucl. Phys. B **229**, 317 (1983)
25. D.G. Richards et al., Fixed order perturbation theory and leading logarithms. Phys. Lett. **136B**, 99 (1984)

26. D.G. Richards et al., Second order corrections to the energy–energy correlation function in quantum chromodynamics. Phys. Lett. **119B**, 193 (1982)
27. Shen-Chang Chao et al., The order α_S^2 energy–energy correlation function at small angles. Nucl. Phys. B **214**, 513 (1983)
28. H.N. Schneider, G. Kramer, G. Schierholz, Higher order QCD corrections to the energy–energy correlation function. Z. Phys. C **22**, 201 (1984)
29. A. Ali, F. Barreiro, An $\mathcal{O}(\alpha\_S^2)$ calculation of energy–energy correlation in e^+e^- annihilation and comparison with experimental data. Phys. Lett. **118B**, 155 (1982)
30. Z. Kunszt et al., QCD at LEP. LEP Physics Workshop Geneva, Switzerland , February 20, 1989, p. 373 (1989)
31. N.K. Falck, G. Kramer, Theoretical studies of energy–energy correlation in e^+e^- annihilation. Z. Phys. C **42**, 459 (1989)
32. E.W.N. Glover, M.R. Sutton, The energy–energy correlation function revisited. Phys. Lett. B **342**, 375 (1995). arXiv:hep-ph/9410234
33. K.A. Clay, S.D. Ellis, A precision calculation of the next-to-leading order energy–energy correlation function. Phys. Rev. Lett. **74**, 4392 (1995). arXiv:hep-ph/9502223
34. G. Kramer, H. Spiesberger, A new calculation of the NLO energy–energy correlation function. Z. Phys. C **73**, 495 (1997). arXiv:hep-ph/9603385
35. A.V. Belitsky et al., Energy–energy correlations in $N = 4$ supersymmetric Yang–Mills theory. Phys. Rev. Lett. **112**, 071601 (2014). arXiv:1311.6800
36. O. Gituliar, S. Moch, Fuchsia and master integrals for energy–energy correlations at NLO in QCD. in 41st International Conference of Theoretical Physics: Matter to the Deepest Kroczyce, Poland, September 4–8, 2017. (2017). Also in preprint arXiv:1711.05549
37. G. Somogyi, Z. Trócsányi, V. Del Duca, A subtraction scheme for computing QCD jet cross sections at NNLO: regularization of doubly-real emissions. JHEP **01**, 070 (2007). arXiv:hep-ph/0609042
38. G. Somogyi, Z. Trócsányi, A subtraction scheme for computing QCD jet cross sections at NNLO: regularization of real-virtual emission. JHEP **01**, 052 (2007). arXiv:hep-ph/0609043
39. T. Becher, M. Neubert, Drell–Yan production at small q_T, transverse parton distributions and the collinear anomaly. Eur. Phys. J. C **71**, 1665 (2011). arXiv:1007.4005
40. I. Moult, H.X. Zhu, Simplicity from recoil: the three-loop soft function and factorization for the energy–energy correlation. (2018). arXiv:1801.02627
41. S. Catani et al., Resummation of large logarithms in e^+e^- event shape distributions. Nucl. Phys. B **407**, 3 (1993)
42. W. Bizon et al., Momentum-space resummation for transverse observables and the Higgs $p_\perp$ at $\mathrm{N^3LL+NNLO}$. (2017). arXiv:1705.09127
43. T. Gehrmann, G. Luisoni, P.F. Monni, Power corrections in the dispersive model for a determination of the strong coupling constant from the thrust distribution. Eur. Phys. J. C **73**, 2265 (2013). arXiv:1210.6945
44. P. Nason, C. Oleari, Next-to-leading order corrections to momentum correlations in $Z^0 \to b\bar{b}$. Phys. Lett. B **407**, 57 (1997). arXiv:hep-ph/9705295
45. K.G. Chetyrkin, R.V. Harlander, J.H. Kuhn, Quartic mass corrections to R_{had} at order $\alpha^3(s)$. Nucl. Phys. B **586**, 56 (2000). arXiv:hep-ph/0005139
46. Particle Data Group, C. Patrignani et al., Review of particle physics. Chin. Phys. C **40**, 100001 (2016)
47. SLD Coll., K. Abe et al., Measurement of $\alpha\_S(M(Z))$ from hadronic event observables at the Z^0 resonance. Phys. Rev. D **51**, 962 (1995). arXiv:hep-ex/9501003
48. L3 Coll., O. Adrian et al., Determination of α_S from hadronic event shapes measured on the Z^0 resonance. Phys. Lett. B **284**, 471 (1992)
49. DELPHI Coll., P. Abreu et al., Determination of α_S in second order QCD from hadronic Z decays. Z. Phys. C **54**, 55 (1992)
50. OPAL Coll., P.D. Acton et al., A determination of $\alpha\_S(M\_Z)$ at LEP using resummed QCD calculations. Z. Phys. C **59**, 1 (1993)
51. OPAL Coll., P.D. Acton et al., An improved measurement of $\alpha\_S(M\_Z)$ using energy correlations with the OPAL detector at LEP. Phys. Lett. B **276**, 547 (1992)
52. TOPAZ Coll., I. Adachi et al., Measurements of α_S in e^+e^- annihilation at $\sqrt{s} = 53.3$GeV and 59.5GeV. Phys. Lett. B **227**, 495 (1989)
53. TASSO Coll., W. Braunschweig et al., A study of energy–energy correlations between 12GeV and 46.8GeV CM energies. Z. Phys. C **36**, 349 (1987)
54. JADE Coll., W. Bartel et al., Measurements of energy correlations in $e^+e^- \to hadrons$. Z. Phys. C **25**, 231 (1984)
55. MAC Coll., E. Fernandez et al., A measurement of energy–energy correlations in $e^+e^- \to$ Hadrons at $\sqrt{s} = 29$GeV. Phys. Rev. D **31**, 2724 (1985)
56. MARKII Coll., D.R. Wood et al., Determination of α_S from energy–energy correlations in e^+e^- annihilation at 29GeV. Phys. Rev. D **37**, 3091 (1988)
57. CELLO Coll., H.J. Behrend et al., Analysis of the energy weighted angular correlations in hadronic e^+e^- annihilations at 22GeV and 34GeV. Z. Phys. C **14**, 95 (1982)
58. PLUTO Coll., C. Berger et al., A study of energy–energy correlations in e^+e^- annihilations at $\sqrt{s} = 34.6$GeV. Z. Phys. C **28**, 365 (1985)
59. PLUTO Coll., C. Berger et al., Energy–energy correlations in e^+e^- annihilation into hadrons. Phys. Lett. **99B**, 292 (1981) **[57(1981)]**
60. L3 Coll., B. Adeva et al., Determination of α_S from energy–energy correlations measured on the $Z0$ resonance. Phys. Lett. B **257**, 469 (1991)
61. OPAL Coll., M.Z. Akrawy et al., A measurement of energy correlations and a determination of $\alpha\_S(M\_Z^0)$ in e^+e^- annihilations at $\sqrt{s} = 91$GeV. Phys. Lett. B **252**, 159 (1990)
62. SLD Coll., K. Abe et al., Measurement of α_S from energy–energy correlations at the Z^0 resonance. Phys. Rev. D **50**, 5580 (1994). arXiv:hep-ex/9405006
63. DELPHI Coll., P. Abreu et al., Consistent measurements of α_S from precise oriented event shape distributions. Eur. Phys. J. C **14**, 557 (2000). arXiv:hep-ex/0002026
64. A. Hoang et al., Precise determination of α_s from the C-parameter distribution. Phys. Rev. D **91**, 094018 (2015). arXiv:1501.04111
65. T. Gleisberg et al., Event generation with SHERPA 1.1. JHEP **02**, 007 (2009). arXiv:0811.4622
66. M. Bahr et al., Herwig++ physics and manual. Eur. Phys. J. C **58**, 639 (2008). arXiv:0803.0883
67. J. Bellm et al., Herwig 7.0/Herwig++ 3.0 release note. Eur. Phys. J. C **76**, 196 (2016). arXiv:1512.01178
68. J. Bellm et al., Herwig 7.1 release note (2017). arXiv:1705.06919 [hep-ph]
69. F. Krauss, R. Kuhn, G. Soff, AMEGIC++ 1.0: a matrix element generator in C++. JHEP **02**, 044 (2002). arXiv:hep-ph/0109036
70. C. Duhr, S. Hoeche, F. Maltoni, Color-dressed recursive relations for multi-parton amplitudes. JHEP **08**, 062 (2006). arXiv:hep-ph/0607057
71. G. Cullen et al., GoSAM-2.0: a tool for automated one-loop calculations within the Standard Model and beyond. Eur. Phys. J. C **74**, 3001 (2014). arXiv:1404.7096
72. T. Sjostrand, S. Mrenna, P.Z. Skands, PYTHIA 6.4 physics and manual. JHEP **05**, 026 (2006). arXiv:hep-ph/0603175
73. J.C. Winter, F. Krauss, G. Soff, A modified cluster hadronization model. Eur. Phys. J. C **36**, 381 (2004). arXiv:hep-ph/0311085

74. J. Bellm, S. Gieseke, S. Plätzer, Merging NLO multi-jet calculations with improved unitarization. Eur. Phys. J. C **78**, 244 (2018). arXiv:1705.06700
75. J. Alwall et al., MadGraph 5: going beyond. JHEP **06**, 128 (2011). arXiv:1106.0522
76. B.R. Webber, A QCD model for jet fragmentation including soft gluon interference. Nucl. Phys. B **238**, 492 (1984)
77. R.A. Fisher, Frequency distribution of the values of the correlation coefficient in samples from an indefinitely large population. Biometrika **10**, 507 (1915)
78. R.A. Fisher, On the probable error of a coefficient of correlation deduced from a small sample. Metron **1**, 3 (1921). http://digital.library.adelaide.edu.au/dspace/bitstream/2440/15169/1/14.pdf
79. F. James, M. Roos, Minuit: a system for function minimization and analysis of the parameter errors and correlations. Comput. Phys. Commun. **10**, 343 (1975)
80. F. James, M. Winkler, MINUIT user's guide. (2004)
81. R.W.L. Jones et al., Theoretical uncertainties on α_S from event shape variables in e^+e^- annihilations. JHEP **12**, 007 (2003). arXiv:hep-ph/0312016
82. Y.L. Dokshitzer, G. Marchesini, B.R. Webber, Nonperturbative effects in the energy energy correlation. JHEP **07**, 012 (1999). arXiv:hep-ph/9905339
83. S. Bethke, α_s 2016. Nucl. Part. Phys. Proc. **282–284**, 149 (2017)